DOI: 10.1021/ic100933t

Inorganic Chemistry
Article

Structure Change Associated with the $[M^{II/III}$ 1,4,7-Triazacyclononane-N,N′,N″-triacetate (TCTA)$]^{-/0}$ Electron Transfers (M = Mn, Fe, and Ni): Crystal Structure for $[Fe^{II}(H_2O)_6][Fe^{II}(TCTA)]_2$

Thomas L. Hatfield,[†,§] Richard J. Staples,[‡] and David T. Pierce*[,†]

[†]*Department of Chemistry, University of North Dakota, Grand Forks, North Dakota 58202, and* [‡]*Department of Chemistry, Center for Crystallographic Research, Michigan State University, East Lansing, Michigan 48824.* [§] *Present Address: 3M Corporation, St. Paul, MN*

Received May 10, 2010

Heterogeneous electron-transfer rate measurements using the scanning electrochemical microscope are reported for the $[M(TCTA)]^{-/0}$ couples (M = Mn, Fe, and Ni) in aqueous solution. Solution IR spectroscopy indicates that N_3O_3 coordination is preserved for each couple within the pH range of 2−4, and susceptibility measurements indicate little or no interference from spin-state changes at room temperature. Marcus−Hush expressions were used to quantitatively relate structural differences between oxidation states to measured standard heterogeneous electron-transfer rate constants. Good correlation was obtained for the Fe couple, and structural changes associated with the Mn and Ni couples were estimated. In addition, the structure of the Fe^{II} complex was determined by X-ray crystallography. The molecule $[Fe(H_2O)_6][Fe(TCTA)]_2$ is trigonal, space group $P3_1/c$ (no. 159) with $a = b = 12.530(3)$ Å, $c = 12.656(4)$ Å, and $Z = 2$. A notable feature of the structure is that the $[Fe(TCTA)]^-$ complex is distributed between two different geometries, one being rigorously trigonal prismatic and the other having a 26° antiprismatic twist.

Introduction

Electron-transfer (ET) reactions involving large (> 20 kJ mol^{-1}) and very small (< 2 kJ mol^{-1}) molecular rearrangements have been extensively investigated since theoretical models by Marcus and Hush provided equations to quantitatively relate structure change and reaction rate.[1−4] Results from this body of work are generally well understood[5] and typically demonstrate that ET kinetics are dominated in the former cases by the activation of major structural change (usually bond dissociation/association)[6−10] and in the latter cases by the dynamics of solvation-sphere reorganization.[11−13]

Less work has traditionally addressed ET reactions that involve moderate structural deformation,[14−17] although this has changed in recent years with the extensive work of Schultz et al.[18−24] Kinetics of these reactions are more

*To whom correspondence should be addressed. E-mail: dpierce@chem.und.edu.

(1) Marcus, R. A. *J. Chem. Phys.* **1956**, *24*, 966–978.
(2) Hush, N. S. *Electrochim. Acta* **1968**, *13*(5), 1005–1023.
(3) Hush, N. S. Parameters of electron-transfer kinetics. In *Mechanistic aspects of inorganic reactions: based on the Conference on Inorganic Reaction Mechanisms at Wayne State University*, Detroit, Michigan, June 10−12, 1981; Endicott, J. F., Rorabacher, D. B., Eds.; American Chemical Society: Washington, DC, 1982.
(4) Sutin, N. *Acc. Chem. Res.* **1982**, *15*(9), 275–282.
(5) Evans, D. H. *Chem. Rev.* **2008**, *108*(7), 2113–2144.
(6) Schultz, F. A., Correlation between structure and heterogeneous electron transfer rates of coordination compounds. In *Molecular electrochemistry of inorganic, bioinorganic, and organometallic compounds*; Pombeiro, A. J. L., McCleverty, J. A., Eds.; Kluwer Academic Press: Dordrecht, The Netherlands, 1993.
(7) Hecht, M.; Schultz, F. A.; Speiser, B. *Inorg. Chem.* **1996**, *35*(19), 5555–5563.
(8) Saveant, J. M. *J. Am. Chem. Soc.* **1987**, *109*(22), 6788–6795.
(9) Pierce, D. T.; Geiger, W. E. *J. Am. Chem. Soc.* **1992**, *114*(15), 6063–6073.
(10) Chin, T. T.; Geiger, W. E.; Rheingold, A. L. *J. Am. Chem. Soc.* **1996**, *118*(21), 5002–5010.
(11) Weaver, M. J. Redox reactions at metal-solution interfaces. In *Electrode Kinetics: Reactions*; Compton, R. G., Ed.; Elsevier: Amsterdam, 1987.
(12) Pyati, R.; Murray, R. W. *J. Am. Chem. Soc.* **1996**, *118*(7), 1743–1749.
(13) Fawcett, W. R.; Opallo, M. *Angew. Chem., Int. Ed. Engl.* **1994**, *33* (21), 2131–2143.
(14) Brunschwig, B. S.; Creutz, C.; MacArtney, D. H.; Sham, T. K.; Sutin, N. *Faraday Discuss.* **1982**, *74*, 113–127.
(15) Szalda, D. J.; Creutz, C.; Mahajan, D.; Sutin, N. *Inorg. Chem.* **1983**, *22*(17), 2372–2379.
(16) Szalda, D. J.; Macartney, D. H.; Sutin, N. *Inorg. Chem.* **1984**, *23*(22), 3473–3479.
(17) Matsumoto, M.; Funahashi, S.; Takagi, H. D. *Z. Naturforsch., B: Chem. Sci.* **1999**, *54*(9), 1138–1146.
(18) Mu, X. H.; Schultz, F. A. *J. Electroanal. Chem.* **1993**, *353*(1−2), 349–355.
(19) Crawford, P. W.; Schultz, F. A. *Inorg. Chem.* **1994**, *33*(19), 4344–4350.
(20) Gao, Y. D.; Lipkowitz, K. B.; Schultz, F. A. *J. Am. Chem. Soc.* **1995**, *117*(48), 11932–11938.
(21) Turner, J. W.; Schultz, F. A. *Inorg. Chem.* **1999**, *38*(2), 358–364.
(22) Turner, J. W.; Schultz, F. A. *J. Phys. Chem. B* **2002**, *106*(8), 2009–2017.
(23) De Alwis, D. C. L.; Schultz, F. A. *Inorg. Chem.* **2003**, *42*(11), 3616–3622.
(24) Lord, R. L.; Schultz, F. A.; Baik, M. H. *J. Am. Chem. Soc.* **2009**, *131* (17), 6189–6197.

 Published on Web 09/24/2010

complex because the barrier-crossing dynamics can be altered by inner-shell bond vibrations that activate structural rearrangement(s),[25,26] and for inorganic systems, the ET can be coupled to changes in metal-centered spin state.[27] Study of these reactions has been hindered by a lack of homologous redox systems that experience variable degrees of mild structural rearrangement,[28] and most have been limited to metal complexes that have N_6 ligand systems (e.g., tris(2,2′-bipyridine), bis(1,4,7,-triazacyclononane), and bis(tris(pyrazol-1-yl)borate)).

A different candidate system encompasses first-row transition metal complexes of the pendent-arm macrocycle 1,4,7-triazacyclononane-N,N′,N″-triacetate ($TCTA^{3-}$). These N_3O_3 complexes have been suggested for investigations of outer-sphere ET since the initial report of their electrochemical behavior by Weighardt and co-workers.[29] Because of a significantly lower field strength compared to N_6 systems, metal complexes with this ligand are usually high-spin at room temperature, and their ET kinetics are not typically complicated by spin-exchange processes. However, their ET kinetics have not yet been evaluated, either through solution exchange or heterogeneous rate measurements.

One mild structural effect associated with $TCTA^{3-}$ complexes is trigonal distortion that results from mutual rotation of the tethered N_3 and O_3 faces.[29,30] Tethering yields the lowest ligand strain when the donor sets are eclipsed in projection along the 3-fold axis of the molecule. Accordingly, complexes of these ligands tend to demonstrate trigonal prismatic geometry with metals that derive no added stabilization from an octhedral field (e.g., high-spin d^5 and d^6).[31,32] Notable examples for $TCTA^{3-}$, its carboxylate derivatives, or its tethered alcohol/alkoxide analogs include high-spin (hs) complexes of Fe^{II} (this work), Fe^{III},[29,33,34] Mn^{II},[30,35] and Co^{II}.[36,37] Metals with other electronic configurations tend to form complexes that reside closer to octahedral geometry. Demonstrated examples include complexes of Cr^{III},[29,34,38] Mn^{III},[39] Mn^{IV},[30,40] Co^{III},[41,42] and Ni^{II}.[40,43,44] These examples clearly indicate that first-row $[M(TCTA)]^{0/-}$ couples possess systematic differences in structure and should be good candidates to probe the effect of mild structural rearrangement on the ET process.

Redox couples that experience little or no structural perturbation generally manifest rapid ET. These systems are prone to erroneous heterogeneous kinetic measurement with solid electrodes when time-based electrochemical techniques, particularly cyclic voltammetry (CV), are employed. Below millisecond time-scales, CV suffers from numerous artifacts associated with current and voltage distortions, particularly solution resistance and double-layer capacitance.[45] These artifacts mimic the effects of sluggish ET in CV traces and can lead to inaccurate rate constant measurements. A more accurate method for the measurement of rapid heterogeneous ET kinetics is scanning electrochemical microscopy (SECM).[46] Remarkably few heterogeneous ET kinetic studies have been performed by SECM, although measurements of inorganic systems have been the most common. These measurements to date include mainly standard redox couples such as $[Fe(H_2O)_6]^{2+/3+}$,[47] $[Ru(NH_3)_6]^{3+/2+}$,[47,48] ferrocene $[Fe(\eta^5\text{-}C_5H_5)_2]^{0/+}$,[49] and several ferrocenyl derivatives.[50−53] Nevertheless, the ferrocene studies are noteworthy because they demonstrate the reliable measurement of an ET rate constant as high as 4 cm s^{-1}, a magnitude not practicable by CV.

This article reports the first detailed ET kinetic measurements of the $[M(TCTA)]^{-/0}$ couples (M = Mn, Fe, and Ni) as well as the use of scanning electrochemical microscopy to perform these measurements. Marcus−Hush expressions were applied to determine if systematic differences in inner-sphere rearrangements are apparent from electrochemical kinetic data and if the differences can be quantitatively related to known structural differences between oxidation states.

Experimental Section

Physical Measurements. ^{1}H NMR spectra were obtained with a Varian VXR 300 MHz instrument; chemical shifts are reported as δ values versus TMS. IR spectra were recorded using a Bio-Rad FTS-40 FTIR. UV−visible spectra were recorded with a Shimadzu UV-260 scanning spectrophotometer. Magnetic moments were measured by a modified Evans method[54] using

(25) Sumi, H.; Marcus, R. A. *J. Chem. Phys.* **1986**, *84*(9), 4894–4914.
(26) Phelps, D. K.; Weaver, M. J. *J. Phys. Chem.* **1992**, *96*(18), 7187–7193.
(27) Turner, J. W.; Schultz, F. A. *Coord. Chem. Rev.* **2001**, *219−221*, 81–97.
(28) Phelps, D. K.; Ramm, M. T.; Wang, Y.; Nelsen, S. F.; Weaver, M. J. *J. Phys. Chem.* **1993**, *97*(1), 181–188.
(29) Wieghardt, K.; Bossek, U.; Chaudhuri, P.; Herrmann, W.; Menke, B. C.; Weiss, J. *Inorg. Chem.* **1982**, *21*(12), 4308–4314.
(30) Belal, A. A.; Chaudhuri, P.; Faillis, I.; Farrugia, L. J.; Hartung, R.; Macdonald, N. M.; Nuber, B.; Peacock, R. D.; Weiss, J.; Wieghardt, K. *Inorg. Chem.* **1991**, *30*(23), 4397–4402.
(31) Wentworth, R. A. D. *Coord. Chem. Rev.* **1972**, *9*(1−2), 171–187.
(32) Hoffmann, R.; Howell, J. M.; Rossi, A. R. *J. Am. Chem. Soc.* **1976**, *98*(9), 2484–2492.
(33) Luckay, R.; Hancock, R. D.; Cukrowski, I.; Reibenspies, J. H. *Inorg. Chim. Acta* **1996**, *246* (1−2 Special Issue), 159−169.
(34) Dixon, D. A.; Shang, M.; Lappin, A. G. *Inorg. Chim. Acta* **1999**, *290* (2), 197–206.
(35) Belal, A. A.; Fallis, I.; Farrugia, L. J.; MacDonald, N. M.; Peacock, R. D. *J. Chem. Soc., Chem. Commun.* **1991**, No. 6, 402–403.
(36) Al-Sagher, H.; Fallis, I.; Farrugia, L. J.; Peacock, R. D. *J. Chem. Soc., Chem. Commun.* **1993**, No. 19, 1499–1500.
(37) Feng, X.-M.; Zhang, Z.; Li, Y.-Z.; Bian, N.-S.; Wang, Z.-L. *Trans. Met. Chem.* (*Dordrecht, Neth.*) **2007**, *32*(1), 95–101.
(38) Farrugia, L. J.; Macdonald, N. M.; Peacock, R. D.; Robb, J. *Polyhedron* **1995**, *14*(4), 541–545.
(39) Fukuda, Y.; Hirota, M.; Kon-No, M.; Nakao, A.; Umezawa, K. *Inorg. Chim. Acta* **2002**, *339*, 322–326.
(40) Fallis, I. A.; Farrugia, L. J.; MacDonald, N. M.; Peacock, R. D. *J. Chem. Soc., Dalton Trans.* **1993**, No. 18, 2759–2763.
(41) Belal, A. A.; Farrugia, L. J.; Peacock, R. D.; Robb, J. *J. Chem. Soc., Dalton Trans.* **1989**, No. 5, 931–935.
(42) Boeyens, J. C. A.; van der Merwe, M. J. *Inorg. Chem.* **1997**, *36*(17), 3779–3780.
(43) van der Merwe, M. J.; Boeyens, J. C. A.; Hancock, R. D. *Inorg. Chem.* **1985**, *24*(8), 1208–1213.
(44) Farrugia, L. J.; Peacock, R. D. *Acta Crystallogr., Sect. C: Cryst. Struct. Commun.* **1991**, *C47*(6), 1312–1313.
(45) Wipf, D. O.; Wightman, R. M. *Anal. Chem.* **1988**, *60*(22), 2460–2464.
(46) Bard, A. J.; Fan, F.-R. F.; Mirkin, M. V. Scanning electochemical microscopy. In *Physical electrochemistry: principles, methods, and applications*; Rubinstein, I., Ed.; M. Dekker: New York, 1995.
(47) Bard, A. J.; Mirkin, M. V.; Unwin, P. R.; Wipf, D. O. *J. Phys. Chem.* **1992**, *96*(4), 1861–1868.
(48) Sun, P.; Mirkin, M. V. *Anal. Chem.* **2006**, *78*(18), 6526–6534.
(49) Mirkin, M. V.; Richards, T. C.; Bard, A. J. *J. Phys. Chem.* **1993**, *97* (29), 7672–7677.
(50) Miao, W.; Ding, Z.; Bard, A. J. *J. Phys. Chem. B* **2002**, *106*(6), 1392–1398.
(51) Taylor, A. W.; Qiu, F.; Hu, J.; Licence, P.; Walsh, D. A. *J. Phys. Chem. B* **2008**, *112*(42), 13292–13299.
(52) Fontaine, O.; Lagrost, C.; Ghilane, J.; Martin, P.; Trippe, G.; Fave, C.; Lacroix, J. C.; Hapiot, P.; Randriamahazaka, H. N. *J. Electroanal. Chem.* **2009**, *632*(1−2), 88–96.
(53) Dumitrescu, I.; Dudin, P. V.; Edgeworth, J. P.; Macpherson, J. V.; Unwin, P. R. *J. Phys. Chem. C* **2010**, *114*(6), 2633–2639.
(54) Sur, S. K. *J. Magn. Reson.* **1989**, *82*(1), 169–173.

a coaxial reference insert (Wilmad WGS-5BL). Conductivity measurements were made using an Amber Science 1054 EC Meter with a 5-mm-diameter × 8 cm flow-through cell standardized with 0.001 M KCl, and elemental analyses were performed by Roberston Microlit Laboratories, Madison, New Jersey. FTIR spectra of D_2O solutions were obtained using a 2-mm-path-length cell with ZnS windows. All complexes were twice evaporated to dryness from D_2O to ensure complete substitution of hydration sphere. Solution pD was monitored with narrow range pH paper (to ±0.1 unit) and adjusted with microliter additions of D_2SO_4 and NaOD solutions.

Materials. Reagent-grade starting materials were used without further purification unless otherwise noted. Water was distilled and then deionized to 18 MΩ cm (Milli-pore).

Syntheses. [Fe(TCTA)] was prepared according to the literature.[29] Preparations of $H_3TCTA \cdot 5H_2O$, $[Fe(H_2O)_6][Fe(TCTA)]_2$, $H_3O[Ni(TCTA)]$, $K[Mn(TCTA)] \cdot H_2O$, and $[Mn(TCTA)] \cdot 3H_2O$ deviated significantly from published procedures, and syntheses of $K[Mn^{III}(TCTA)(OH)] \cdot H_2O$ and $[Ni(TCTA)] \cdot 3H_2O$ were original to this work.[55]

$H_3TCTA \cdot 5H_2O$. A 50 mL aqueous solution containing bromoacetic acid (3.9 g, 28 mmol) and KOH (1.6 g, 28 mmol) was added with stirring to an aqueous solution containing 1,4,7-triazacyclononane (1.2 g, 9 mmol) at 0 °C (ice bath). After heating to 80 °C, a concentrated solution of KOH was added dropwise until the pH remained at 9 for 5 min. Volume was reduced under a vacuum to ca. 8 mL, and the solution was acidified to pH 3 with concentrated hydrobromic acid. The tris-acid was isolated as the second fraction from an ion retardation column (3 × 62 cm, Bio-Rad AG 11A8, 50−100 mesh) using water as the eluent. Evaporation gave the colorless product as a clear glass. The yield was 1.7 g (66%). ^1H NMR (D_2O): δ 2.8 (s, 12H, N−CH_2−CH_2−N), δ 3.8 (s, 6H, N−CH_2−COO). Anal. Calcd for $C_{12}H_{21}N_3O_6 \cdot 5H_2O$ (393.40 g mol^{-1}): C, 36.64; H, 7.94; N, 10.68. Found: C, 37.10; H, 8.14; N, 10.44.

$[Fe^{II}(H_2O)_6][Fe^{II}(TCTA)]_2$. Under Schlenk conditions and using only degassed solutions, anhydrous $FeCl_2$ (0.0867 g, 0.68 mmol) was added to an aqueous 5 mL solution of $H_3TCTA \cdot 5H_2O$ (0.2437 g, 0.62 mmol). The pH was adjusted to 8 with a 25% solution of $[(CH_3CH_2)_4N]OH$ and after 15 min was adjusted again to a pH of 6 with concentrated H_2SO_4. After the addition of 10 mL of dry ethanol, the solution was filtered, and a number of air-sensitive, colorless needles formed upon standing. The yield was 0.059 g (22%). IR (KBr pellet): ν(C═O, COOM), 1600 cm^{-1}. For solutions up to 10 mM, there was no absorbance detected over the 190−800 nm range of the UV−visible spectrum. Anal. Calcd for $C_{24}H_{48}N_6O_{18}Fe_3$ (876.35 g mol^{-1}): C, 32.89; H, 5.52; N, 9.59. Found: C, 32.91; H, 5.64; N, 9.60.

$K[Mn^{II}(TCTA)] \cdot H_2O$. Under Schlenk conditions and using only degassed solutions, $Mn(ClO_4)_2 \cdot 6H_2O$ (2.62 g, 7.25 mmol) was added to a 5 mL aqueous solution of $H_3TCTA \cdot 5H_2O$ (2.2 g, 7.25 mmol). ***Caution!*** *Perchlorate salts are potentially explosive.* The solution was heated to 50 °C, and the pH was adjusted to 7 with a 2 M KOH solution. After cooling, the complex was isolated as the first fraction from the ion retardation column using degassed water as the eluent. Evaporation gave the colorless product as a clear glass. The yield was 1.5 g (58%). Molar conductance: 119.5 cm^{-1} mol^{-1} Ω^{-1} (2 ions). IR (KBr pellet): ν(C═O, COO−M), 1580 cm^{-1}. For solutions up to 10 mM, there was no absorbance over the 190−800 nm range of the UV−visible spectrum. Magnetic susceptibility: μ_{eff} 5.9 (5 unpaired electrons). Anal. Calcd for $K[C_{12}H_{18}N_3O_6Mn] \cdot H_2O$ (412.43 g mol^{-1}): C, 34.95; H, 4.89, N, 10.19. Found: C, 34.85; H, 4.92; N, 10.05.

$[Mn^{III}(TCTA)] \cdot 3H_2O$. Synthesis was performed by chemical oxidation of $K[Mn^{II}(TCTA)]$ (0.5 g 1.1 mmol) at 70 °C using $K_2S_2O_8$ (0.3 g, 1.1 mmol) in 5 mL of water. After 10 min, the reaction mixture was cooled and the product was isolated as the first fraction from the ion retardation column using water as the eluent. Evaporation gave a red oil that was extracted for 4 h with 20 mL of purified CH_3CN. Evaporation of the extracts under a high vacuum gave the product as a red glass. Yield was 0.15 g (30%). Molar conductance: 12.7 cm^{-1} mol^{-1} Ω^{-1} (no ions). IR (KBr pellet) ν(C═O, COO−M): 1650 cm^{-1}. UV−visible (H_2O): λ_{max} 470 nm (ε_{470} 1080 L mol^{-1} cm^{-1}). Magnetic susceptibility: μ_{eff} 5.0 (4 unpaired electrons). Anal. Calcd. for $[C_{12}H_{18}N_3O_6Mn] \cdot 3H_2O$ (355.23 g mol^{-1}): C, 35.22; H, 5.11; N, 10.26. Found: C, 34.96; H, 4.95; N, 10.07.

$K[Mn^{III}(TCTA)(OH)] \cdot H_2O$. Unextracted portions of the oil isolated in the preceding synthesis consistently showed IR evidence of a second product. Dissolution of the remaining oil in water followed by re-elution on the ion-retardation column yielded a second product that was distinct from $[Mn^{III}TCTA]$. Molar conductance: 118.2 cm^{-1} mol^{-1} Ω^{-1} (2 ions). IR (KBr pellet): ν(C═O, COO−M), 1650 cm^{-1}, ν(C═O, COOH), 1710 cm^{-1}. UV−visible, (H_2O), λ_{max}: 470 nm (ε_{470} 740 L mol^{-1} cm^{-1}), 480 nm (sh) (ε_{480} ca. 700 L mol^{-1} cm^{-1}). Magnetic susceptibility μ_{eff}: 4.9 (4 unpaired electrons). Anal. Calcd. for $K[C_{12}H_{19}N_3O_7Mn] \cdot H_2O$ (429.40 g mol^{-1}): C, 33.54; H, 4.93; N, 9.78. Found: C, 33.37; H, 5.20; N, 9.71.

$H_3O[Ni^{II}(TCTA)] \cdot H_2O$. $Ni(ClO_4)_2 \cdot 6H_2O$ (0.74 g, 2.0 mmol) was added to a 10 mL aqueous solution of $H_3TCTA \cdot 5H_2O$ (1.53 g, 3.88 mmol), and the mixture was stirred while heating to 80 °C. KOH solution was added in drops over a 20 min period to maintain a neutral pH. After cooling, 60 mL of ethanol was added, and the supernate was evaporated under a high vacuum to yield an impure potassium salt of the complex. The solid was dissolved in a minimum of water, acidified to pH 3 with concentrated sulfuric acid, and eluted with water on the ion retardation column. Evaporation of the first fraction gave the pure product as a violet glass. The yield was 0.38 g (48%). Molar conductance: 121.2 cm^{-1} mol^{-1} Ω^{-1} (2 ions). IR (KBr pellet): ν(C═O, COOM), 1580 cm^{-1}. UV−visible (H_2O), λ_{max}: 350 nm (ε_{350} 18 L mol^{-1} cm^{-1}), 570 nm (ε_{570} 13 L mol^{-1} cm^{-1}). Magnetic susceptibility μ_{eff} = 2.8 (2 unpaired electrons). Anal. Calcd for $H_3O[C_{12}H_{18}N_3O_6Ni] \cdot H_2O$ (396.04 g mol^{-1}): C, 36.39; H, 5.85; N, 10.61. Found: C, 36.34; H, 6.16; N, 10.35.

$[Ni^{III}(TCTA)] \cdot 3H_2O$. A cursory preparation and crystallographic structure of this complex appeared in a communication in 1983.[56] However, the isolated crystals were later identified as $[Co^{III}(TCTA)]$.[42] While a similar route was use to prepare the Ni^{III} complex in this work (oxidation of the Ni^{II} complex with nitric acid), more extensive characterization was performed to identify of the compound. A second desalting fraction from the preceding synthesis of the Ni^{II} complex was evaporated to 5 mL and acidified to pH 3 with concentrated HNO_3. The violet solution was allowed to stand at room temperature for 7 days, after which a small number of lavender crystals were isolated. The yield was 0.049 g (6.8%, based on $Ni(ClO_4)_2 \cdot 6H_2O$ used in preceding synthesis). IR (KBr pellet): ν(C═O, COOM), 1620 cm^{-1}. UV−visible (H_2O), λ_{max}: 285 nm (ε_{350} 1270 L mol^{-1} cm^{-1}). Magnetic susceptibility μ_{eff}: 3.7 (3 unpaired electrons). Anal. Calcd. for $[C_{12}H_{18}N_3O_6Ni] \cdot 3H_2O$ (413.03 g mol^{-1}): C, 34.89; H, 5.86; N, 10.17. Found: C, 34.95; H, 6.47; N, 9.84.

Electrochemistry. Apparatus and materials used for conventional CV (up to 20 V s^{-1}), chronoamperometry, and bulk coulometry have been described.[57] Diffusion coefficients (D) for each $M^{II/III}$ couple were determined by performing chronoamperometry

(55) Hatfield, T. L. Synthesis, characterization and electrochemical investigations of metal complexes derived from pendant-arm macrocycles. Ph. D. Dissertation, 1997.

(56) van der Merwe, M. J.; Boeyens, J. C. A.; Hancock, R. D. *Inorg. Chem.* **1983**, *22*(24), 3489–3490.

(57) Pierce, D. T.; Hatfield, T. L.; Joseph Billo, E.; Ping, Y. *Inorg. Chem.* **1997**, *36*(14), 2950–2955.

before and after bulk coulometry. Fast scan CV was performed with a home-built three-electrode potentiostat having a minimum rise-time of 300 ns. Voltage ramps were applied with a 0−30 MHz function generator (Krohn-Hite 2400), and CV traces were acquired with a 400 MHz digital storage oscilloscope (LeCroy 9040A). Gold and platinum ultramicroelectrodes (UMEs) were fabricated with 125, 50, 25, and 10-μm-diameter wire as described by Pierce et al.[58] UMEs were polished with 0.05 μm alumina (Buehler), washed copiously with water, and wiped dry prior to use. Uncompensated solution resistance was not measured, and solution resistance compensation was not employed. Solution resistance effects were minimized by matching electrode size to scan rate using the guidelines of Evans et al.[59]

Solutions of water (18 MΩ cm, Milli-pore) or water with acetonitrile (HPLC grade) with either 0.10 M ammonium perchlorate (NH_4ClO_4) or 0.10 M tetra(N-ethyl)ammonium perchlorate (TEAP) as a supporting electrolyte were brought to a pH of 3−4 by small additions of perchloric acid. Voltages recorded in aqueous solution were referenced to the saturated calomel electrode (SCE) to a precision of ±10 mV. Voltages recorded in acetonitrile and in acetonitrile/water mixtures were referenced to the ferrocene/ferroncenium ($Fc^{0/+}$) couple, which was added to the solution as an internal standard. All measurements were performed at ambient temperature (23 ± 2 °C).

The system used to perform SECM measurements has been thoroughly described.[55] Briefly, the cell was a Teflon cylinder compressed (via O-ring) against a gold-coated glass plate. The plate acted as both the cell bottom and substrate electrode. The top of the cell was fitted with a plastic cap that was drilled to accept a platinum wire auxiliary electrode, a fritted silver quasi-reference electrode, an argon purge tube, and a probe UME. The entire cell was bolted rigidly to a horizontal translation stage that was adjustable in two dimensions with manual micrometers (Edmond Scientific). The 10 and 25-μm-diameter UMEs used for SECM were disk-shaped electrodes with the glass beveled to achieve a tip radius (d) that was 10 times the wire radius (a) (i.e., $d/a = 10$). The probe UME was held rigidly to a double-hinge mirror mount (Edmond Scientific) that kept the UME perpendicular to the substrate electrode. The mount was in turn bolted to a vertical translation stage (Burleigh Instruments). In this manner, the vertical position of the UME could be moved several centimeters with a precision of ±0.01 μm using a model IW-700 piezoelectric inch-worm translator (PZT) and model 6000 controller (Burleigh Instruments). The controller was interfaced to a microcomputer using the program CE_6000.[60] The same program permitted simultaneous acquisition of electrochemical data from a home-built bipotentiostat via an analog−digital conversion card (DT-2821, Data Translation). The bipotentiostat controlled the four electrodes of the EM cell, and a TTL-triggered function generator (Leader Instruments) provided variable-frequency triangle ramps to perform CV at either the probe or the substrate electrode.

Crystal Data and Intensity Measurements for $[Fe(H_2O)_6][Fe(TCTA)]_2$. A colorless needle (0.25 × 0.25 × 0.10 mm) obtained from ethanol/water media was chosen for X-ray diffraction (XRD) analysis and mounted on a glass fiber using grease. A data set ($3.76 < 2\theta < 56.42°$, $-13 \le h \le 16$, $-16 \le k \le 12$, and $-16 \le l \le 14$) of 1271 frames with a final resolution of 0.75 Å was collected at 213 K with a Siemens SMART CCD diffractometer equipped with an LT-2 low-temperature apparatus. Omega scans of 0.3° per frame for 30 s were used such that a hemisphere was collected. The first 50 frames were recollected at the end of data collection to monitor for decay. Of 8548 reflections measured, 2502 independent reflections gave $R_{int} = 0.0347$. Cell parameters were retrieved using SMART software and refined using SAINT software on all observed reflections.[61] Data reduction was performed using SAINT, which corrects for Lp and decay. Absorption corrections were applied using SADABS[62] supplied by George Sheldrick. The structure was solved by the direct method using the SHELXS-97 program and refined by least-squares method on F^2, SHELXL-97, incorporating SHELXTL-PC version 5.03.[63] All non-hydrogen atoms were refined anisotropically. Hydrogens were calculated by geometrical methods and refined as a riding model. A final difference map showed no rest-electron density greater than $0.460e$ Å^{-3} or less than $-0.646e$ Å^{-3}. The crystal used for the diffraction study showed no decomposition during the data collection. Crystal data and additional details of the collection are contained in Table 1. Selected bond lengths and angles are given in Table 2.

Table 1. Crystallographic Data for $[Fe^{II}(H_2O)_6][Fe^{II}(TCTA)]_2$

chemical formula	$C_{24}H_{48}Fe_3N_6O_{18}$
fw	876.23
space group	$P3_1/c$ (No. 159)
cryst syst	trigonal
lattice constants	
a, Å	12.530(3)
b, Å	12.530(3)
c, Å	12.656(4)
V, Å^3	1720.6(7)
Z	2
ρ_{calcd}, g cm^{-3}	1.691
λ, Å	0.710 73
T, K	213(2)
μ, cm^{-1}	13.38
$R(F)^a$	0.0275
$R_w(F^2)^b$	0.0331

$^a R = \sum||F_o| - |F_c||/\sum|F_o|$. $^b R_w = [\sum[w(F_o^2 - F_c^2)^2]/\sum[w(F_o^2)^2]]^{1/2}$; $w = 1/[\sigma^2(F_o)^2 + (0.0232P)^2 + 0.9766P]$ where $P = (F_o^2 + 2F_c^2)/3$.

Results and Discussion

Coordination in Solution. Carbonyl bands in the IR spectra of $TCTA^{3-}$ complexes were effective indicators of pendent-arm displacement and/or metal oxidation state. Spectra recorded at different solution pD values were used to identify conditions that preserved N_3O_3 coordination of TCTA for both oxidation states of each couple.[55] None of the six isolated $[M(TCTA)]^{-,0}$ complexes showed evidence of acetate displacement, substitution, or decomposition within the pD range of 3 to 5. UV−visible spectra also showed little change over a similar pH range. Most complexes dissociated below a pD of 2 with precipitation of H_3TCTA. At pD's above 6, hydroxide substitution of one acetate arm occurred with $[Ni(TCTA)]^-$ and $[Mn(TCTA)]^{-,0}$, while [Fe(TCTA)] demonstrated complete decomplexation followed by precipitation of ferric hydroxide. The more reactive [Ni(TCTA)] species showed rapid decomposition above a pD of 5, as reported by de Castro et al.[64] Observations of acetate displacement by IR were particularly important to the subsequent electrochemical study of the Mn system because the

(58) Pierce, D. T.; Unwin, P. R.; Bard, A. J. *Anal. Chem.* **1992**, *64*(17), 1795–1804.
(59) Bowyer, W. J.; Engelman, E. E.; Evans, D. H. *J. Electroanal. Chem.* **1989**, *262*(1−2), 67–82.
(60) Wipf, D. O. *CE_6000, Program for automation of the Burleigh 6000 piezoeletric controller*; Mississippi State University: Mississippi State, MS, 1994.
(61) *SMART*; *SAINT*, v. 4.043; Siemens Analytical Instruments Division: Madison, WI, 1995.
(62) SADABS Program for absorption corrections using Bruker-AXS CCD based on the method of Robert Blessing: Blessing, R. H. *Acta Crystallogr., Sect. A* **1995**, *A51*, 33−38.
(63) Sheldrick, G. M. *Acta Crystallogr., Sect. A: Found. Crystallogr.* **2008**, *A64*(1), 112–122.
(64) de Castro, B.; Gomes, J.; Marques, M. P. M.; Geraldes, C. F. G. C. *J. Chem. Soc., Dalton Trans.* **1995**, *12*, 2041–2044.

Table 2. Selected Bond Lengths and Angles for $[Fe^{II}(H_2O)_6][Fe^{II}(TCTA)]_2$

Bond Lengths (Å)					
Fe1 System					
Fe1−O1	2.091(2)	N1−C3	1.549(6)	C3−C4	1.471(6)
Fe1−N1	2.210(3)	N1−C3B[a]	1.486(6)	C3B−C4[a]	1.617(7)
Fe11 System					
Fe11−O11	2.0844(18)	N11−C13	1.463(3)	C13−C14	1.524(4)
Fe11−N11	2.184(2)				
Fe2 System					
Fe2−O3	2.1491(19)				
Fe2−O4	2.124(2)				
Bond Angles (deg)					
Fe1 System					
O1−Fe1−O1a	91.23(9)	N1−C3−C4	110.4(4)		
O1−Fe1−N1	76.86(9)	N1−C3B−C4[a]	106.0(4)		
N1−Fe1−N1a	79.40(10)	C3−C4−O1	114.0(3)		
O1−Fe1−N1a	133.40(11)	C3B−C4−O1[a]	111.3(3)		
Fe11 System					
O11−Fe11−O11e	94.32(7)	N11−C13−C14	110.3(2)		
O11−Fe11−N11	76.94(8)	C13−C14−O11	117.4(2)		
N11−Fe11−N11e	81.47(9)				
O11−Fe11−N11e	151.13(8)				
Fe2 System					
O3−Fe2−O3c	87.61(8)	O3−Fe2−O4	179.25(8)		

[a] Value for 48% disordered form.

pentadentate complex $[Mn^{III}(TCTA)(OH)]^-$ was found to readily and irreversibly adsorb to gold electrodes. This effect was confirmed with the isolated compound, $K[Mn^{III}(TCTA)(OH)]\cdot H_2O$.

General Electrochemical Behavior. Formal potentials of the $[M(TCTA)]^{-/0}$ couples generally corresponded to values first reported by Weighardt et al.[29] Changes in concentration (0.05 to 0.5 M) of ammonium or tetraethylammonium perchlorate electrolytes did not shift these formal potentials more than 20 mV, indicating little or no ion pairing effects. Characteristics determined by bulk coulometry with solution pH values between 3 and 5 were a transfer of 1.00 ± 0.02 e^- equiv mol^{-1} for each couple and chemical stability exceeding 1 min. Fast scan CV indicated diffusion-controlled behavior of each couple with no evidence of structural intermediates up to a sweep rate of 50 kV s^{-1}. These characteristics permitted the uncomplicated study of ET kinetics by CV and SECM, even for the extremely positive $[Ni(TCTA)]^{-/0}$ couple at $E_{1/2} = 0.90$ V versus SCE in water solution.

The Mn system demonstrated several unusual features not previously reported. A $[Mn(TCTA)]^{0/+}$ couple at $E_{1/2} = 0.68$ V vs SCE was found to be 380 mV more positive than that of the $[Mn(TCTA)]^{-/0}$ couple in water solutions. This difference in formal potentials is surprisingly small compared to those of N_6 and N_4O_2 ligand systems (ca. 1 V),[65−67] but it is more common for cofacial N_3O_3 systems.[30,68] Equivalent current plateaus of stirred solution voltammograms and equal peak heights of differential-pulse voltammograms confirmed the same 1 e^- equiv mol^{-1} stoichiometry for both $Mn^{II/III}$ and $Mn^{III/IV}$ couples. Although CV traces (Figure 1) indicated nearly Nernstian behavior of the $Mn^{III/IV}$ couple ($\Delta E_{p,III/IV}$ = 70 mV at 0.2 V s^{-1}), the $Mn^{II/III}$ couple demonstrated sluggish behavior even at low sweep rates ($\Delta E_{p,II/III}$ = 138 mV at 0.2 V s^{-1}).

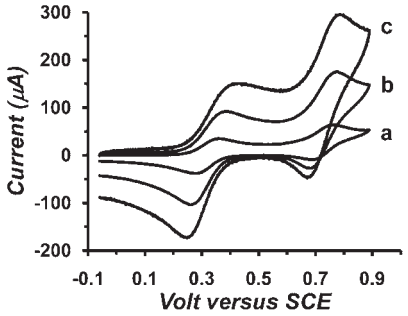

Figure 1. CV of the $[Mn(TCTA)]^{-/0/+}$ couples in water with 0.5 M NH_4ClO_4 (pH 3.6) recorded at a Pt disk electrode. Traces were recorded with sweep rates of (a) 0.25, (b) 2, and (c) 6 V s^{-1}.

The $[Mn(TCTA)]^{-/0/+}$ system was also affected by electrode blocking at elevated pH. Irreversible adsorption of a partially hydrolyzed form of the Mn^{III} complex was suspected to cause this blocking because similar, severe adsorption was also observed with the isolated $[Mn(TCTA)(OH)]^-$complex. No electrode blocking was detected for the $[Mn(TCTA)]^{-/0/+}$ system between a pH of 3 and 4, even at UMEs used for SECM.

Structure of $[Fe^{II}(H_2O)_6][Fe^{II}(TCTA)]_2$. To quantify the structural rearrangements associated with each $[M(TCTA)]^{-/0}$ couple, numerous attempts were made to obtain X-ray-quality crystals for undocumented $[M(TCTA)]^{-,0}$ structures (M = Fe^{II}, Mn^{II}, Mn^{III}, and Ni^{III}). Only attempts with the Fe^{II} complex were successful. This structure (Figure 2) presented several interesting features.

Most striking was the presence of two different geometrical forms of the $[Fe(TCTA)]^-$ complex. One form had rigorously trigonal prismatic geometry (Fe1 system, Figure 3), while the other had a 26° antiprismatic twist (Fe11 system, Figure 4). The lattice also contained octahedral $[Fe(H_2O)_6]^{2+}$ counterions (designated as Fe2 system). The prismatic Fe1 system was stacked with the counterion along the 3-fold axis. While there was little evidence of hydrogen bonding between the Fe1 and Fe2 systems (O1−O4 4.19 Å and O2−O4 5.96 Å), carbonyl oxygens of the Fe11 system did present favorable bonding distances to waters of the counterion (O12−O3 2.77 Å). The prismatic Fe1 system showed a nearly 1:1 disorder of the acetate arms and ethylene bridges that apparently corresponded to two unique ligand conformations. Attempts to solve and refine in the centrosymmetric space group failed to give satisfactory results. The 48% form of the Fe1 system (semitransparent spheres/bonds in Figures 2 and 3) showed δ conformations for the acetate arms

(65) Biswas, S.; Mitra, K.; Chattopadhyay, S. K.; Adhikary, B.; Lucas, C. R. *Trans. Met. Chem.* **2005**, *30*(4), 393–398.
(66) Hossain, F.; Rigsby, M. A.; Duncan, C. T.; Milligan, P. L., Jr.; Lord, R. L.; Baik, M. H.; Schultz, F. A. *Inorg. Chem.* **2007**, *46*(7), 2596–2603.
(67) Mitra, K.; Biswas, S.; Lucas, C. R.; Adhikary, B. *Inorg. Chim. Acta* **2006**, *359*(7), 1997–2003.
(68) Auerbach, U.; Eckert, U.; Wieghardt, K.; Nuber, B.; Weiss, J. *Inorg. Chem.* **1990**, *29*(5), 938–944.

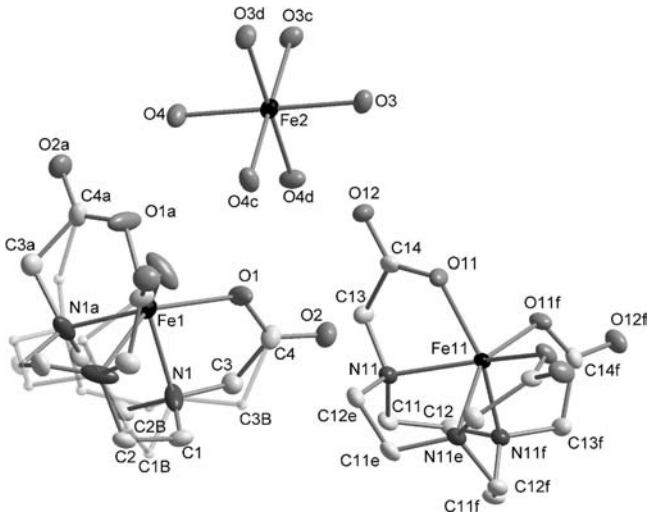

Figure 2. Diagram with 50% probability thermal ellipsoids showing the atom number scheme for the trigonally symmetric structure of $[Fe^{II}(H_2O)_6]$-$[Fe^{II}(TCTA)]_2$. The semitransparent spheres/bonds illustrate a 48% disordered form of the prismatic Fe11 system.

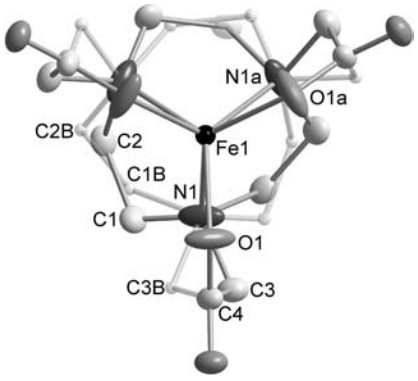

Figure 3. Diagram showing a C_3 perspective for the disordered Fe1 system of $[Fe^{II}(H_2O)_6][Fe^{II}(TCTA)]_2$. Ellipsoids show the 52% disordered form (λ conformations of endo- and exocyclic carbon bridges), and semitransparent spheres/bonds show the 48% disordered form (δ conformations of endo- and exocyclic carbon bridges).

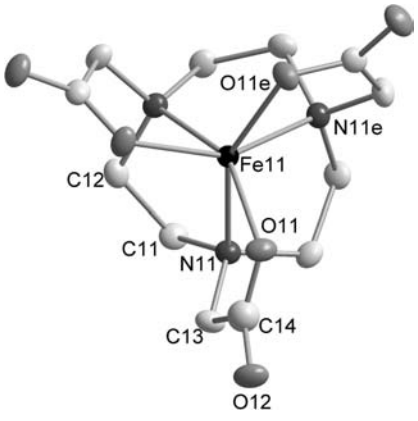

Figure 4. Diagrams showing a C_3 perspective for the Fe11 system of $[Fe^{II}(H_2O)_6][Fe^{II}(TCTA)]_2$.

and ethylene bridges of the ligand. These same conformations were present in the Fe11 system. The 52% form of the Fe1 system (ellipses in Figures 2 and 3) showed λ conformations for acetates and ring ethylenes of TCTA. This configuration has been reported previously by Weighardt et al. for the $[Fe^{III}(TCTA)]^0$ complex.[29]

Structure Change Associated with $[M(TCTA)]^{-/0}$ Couples. The extent that structural rearrangement perturbs each $[M(TCTA)]^{0/-}$ couple during ET was estimated from XRD data compiled for each metal with $TCTA^{3-}$ or analogous N_3O_3 ligands (Table 3). Although solid-state data must be used with caution when inferring metal coordination and ligand conformation in solution, the approach is generally valid provided that no coordinate bonds are broken or drastically rearranged when a complex is solvated.[69] IR studies of $[M(TCTA)]^{0,-}$ solutions provided this evidence in the present study.

Data compiled in Table 3 indicate that the $[Fe(TCTA)]^{-/0}$ couple experiences small metal−ligand bond length changes and maintains the same, nearly prismatic geometry. Unlike N_6 complexes, the $[Fe(TCTA)]^{-/0}$ couple with its relatively weak N_3O_3 ligand field does not experience a spin-state change. These properties are expected to result, respectively, in small contributions to the inner-sphere activation enthalpy and entropy of the ET process.

A comparable estimate of the $[Mn(TCTA)]^{-/0}$ structural change is not possible because crystallographic data have not been reported for either species of the $Mn^{II/III}$ couple. However, other data in Table 3 are noteworthy. First, structures for Mn^{II} and Mn^{IV} complexes with three different alcohol-pendent ligands (H_3TCTHE, H_3TCTHP, and H_3TCTHB) have been determined. All three N_3O_3 ligands demonstrate remarkably similar octahedral structures with Mn^{IV}, and the H_3TCTHP ligand maintains a prismatic geometry around Mn^{II} whether it is hydrogen-bound as a dimer or not. Second, Fe and Ni complexes with these same alcohol ligands show very similar structures to their $TCTA^{3-}$ counterparts—even when the alkoxide groups are protonated.

On the basis of these characteristics, data for the $[Mn(TCTHP)]^{-/0/+}$ system should provide some insight regarding structural changes associated with the $[Mn(TCTA)]^{-/0/+}$ system. Most outstanding are the substantial twist angle and metal−ligand bond length differences between Mn^{II} and Mn^{IV} oxidation states. The relatively sluggish CV responses shown by Belal et al. for the $[Mn(TCTHP)]^{-/0}$ couple[30] and noted in this study for the $[Mn(TCTA)]^{-/0}$ couple strongly suggest that a greater part of $Mn^{II,IV}$ structure change occurs with the $Mn^{II/III}$ process. LFSE arguments support this suggestion[31] as does the structure published for a Mn^{III} 1′-propionate derivative.[39] With greater flexibility provided by an additional methylene in the carboxylate pendent arms, this Mn^{III} complex resides closer to octahedral geometry than even the Mn^{IV} alcohol complexes while adopting M−N and M−O bond distances that are intermediate between those of Mn^{II} and Mn^{IV} alcohol complexes. Remarkably, this high-spin Mn^{III} complex demonstrates normal and *equivalent* lengths for Mn−N bonds (2.123 Å) and Mn−O bonds (1.973 Å) in the solid state even though this center should experience strong Jahn−Teller distortion.[39] The same structural anomaly has been reported for a N_3O_3 Schiff-base ligand complex.[70] Although Jahn−Teller

(69) Martell, A. E. *Mater. Chem. Phys.* **1993**, *35*(3−4), 273–280.
(70) Alcock, N. W.; Cook, D. F.; McKenzie, E. D.; Worthington, J. M. *Inorg. Chim. Acta* **1980**, *38*(C), 107–112.

Table 3. Twist Angles (ϕ), Average Metal−Ligand Bond Lengths (a), and Ring Conformations Determined by XRD for N-Pendent 1,4,7-Triazacyclononane Complexes $[M^{II,III,IV}(N_3O_3)]^{-,0,+}$ (M = Mn, Fe, Ni)

M	L[a]	conf.[b]	ϕ[c] (deg)	$\Delta\phi$ (deg)	a_{M-N} (Å)	Δa_{M-N} (Å)	a_{M-O} (Å)	Δa_{M-O} (Å)	ref
Fe^{II}	TCTA	$\lambda\lambda$	60		2.21		2.09		*d*
Fe^{II}	TCTA	$\delta\delta$	34		2.18		2.08		*e*
Fe^{III}	TCTA	$\lambda\lambda$	35		2.18		1.96		29
Fe^{III}	TCTPr2	$\lambda\lambda$	34		2.17		1.95		34
Fe^{III}	TCTHE[f]	$\delta\lambda$	41		2.15		1.95		33
$Fe^{II/III}$	TCTA	$\lambda\lambda$		−25		−0.03		−0.13	
Mn^{II}	TCTHP[f]	$\lambda\delta$	37		2.25		2.17		30
Mn^{II}	TCTHP[f]	$\delta\delta$	60		2.25		2.14		30, 35
Mn^{III}	TCTPr1	$\delta\lambda$	3		2.12		1.97		39
Mn^{IV}	TCTHE	$\lambda\delta$	9		2.04		1.84		30
Mn^{IV}	TCTHP[f]	$\lambda\delta$	11		2.05		1.86		30, 35
Mn^{IV}	TCTHB	$\delta\lambda$	11		2.05		1.83		40
$Mn^{II,IV}$	TCTHP	$\lambda\delta$		−26		−0.20		−0.31	
Ni^{II}	TCTA	$\delta\lambda$	12		2.04		2.08		43
Ni^{II}	TCTHP[f]	$\lambda\delta$	18		2.06		2.08		44
Ni^{II}	TCTHB[f]	$\delta\lambda$	18		2.05		2.09		40

[a] Ligand abbreviations: TCTA = 1,4,7-triazacyclononane-*N*,*N*′,*N*″-triacetate, TCTPr1 = 1,4,7-triazacyclononane-*N*,*N*′,*N*″-[1-propionate], TCTPr2 = 1,4,7-triazacyclononane-*N*,*N*′,*N*″-[(2*R*)-2-propionate], TCTHE = *N*,*N*′,*N*″-tris(2-hydroxyethyl)-1,4,7-triazacyclononane, TCTHP = *N*,*N*′,*N*″-tris[(2*S*)-2-hydroxypropyl]-1,4,7-triazacyclononane, TCTHB = *N*,*N*′,*N*″-tris[(2*R*)-2-hydroxy-3-methylbutyl]-1,4,7-triazacyclononane. [b] Configurations of endocyclic (ethylene) and exocyclic (pendent) rings, respectively.[30] [c] Defined as twist *away* from ideal octahedral coordination (0° octahedron, 60° prismatic). [d] Data reported in this work for 52% disordered Fe1 system (Figure 3). [e] Data reported in this work for Fe11 system (Figure 4). [f] Crystallized with pendent alcohol ligands either partially protonated as a hydrogen-bonded dimer or fully protonated.

distortions should presumably influence both high-spin $Mn^{II/III}$ and $Mn^{III/IV}$ couples, facially tethered N_3O_3 ligands may create a disproportionate structural change with the $Mn^{II/III}$ process.

The lack of crystallographic data for the $[Ni^{III}(TCTA)]^0$ complex or N_3O_3 analogs complicates the assessment of structural change for the $[Ni(TCTA)]^{-/0}$ couple. As with the $[Fe(TCTA)]^{-/0}$ couple, LFSE calculations predict very little geometric change between these oxidation states,[31] and physical data indicate no change in spin-state. Because Jahn−Teller distortions are also weak in both high-spin systems, it seems reasonable to expect low inner-sphere barriers for both $[Ni(TCTA)]^{-/0}$ and $[Fe(TCTA)]^{-/0}$ couples. A more quantitative assessment was obtained by acquiring ET rate constants and estimating inner-sphere barriers through Marcus−Hush expressions.

SECM Measurements of ET Kinetics. Measurements were performed by precisely lowering a beveled ultramicroeletrode (UME) tip to within fractions of a micrometer from a substrate electrode. Application of appropriate voltages to both the UME and the substrate electrode caused diffusive cycling of the tested redox couple within the small interelectrode gap (d). SECM voltammograms of the $[Ni(TCTA]^{-/0}$ couple (Figure 5) demonstrated that larger UME currents were produced by more rapid recycling within smaller gaps.

Because gap size governs the effective time-scale of the SECM measurement, it affects both kinetic resolution and accuracy. Gaps as small as 0.10 ± 0.05 μm can be obtained, which allow travel times as short as 10 μs between opposing electrodes. Achieving a similar time-scale by fast scan CV would require a sweep rate above 20 kV s^{-1}. Unlike CV, SECM kinetic measurements are made under steady-state conditions because a reaction−diffusion competition is rapidly enforced within the gap. Because slower redox couples manifest lower steady-state UME currents near their standard potential, apparent standard heterogeneous rate constants ($k_{ET,app}$) and transfer coefficients (α_{app}) can be extracted from $E_{1/4}$, $E_{1/2}$, and

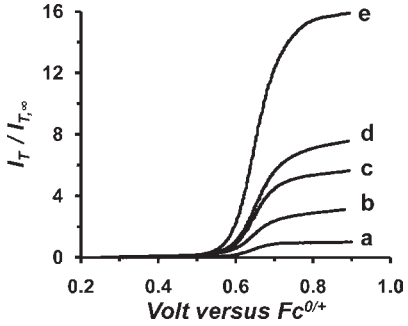

Figure 5. Linear sweep voltammograms (0.020 V s^{-1}) of the $[Ni(TCTA)]^{-/0}$ couple in 85% water/acetonitrile with 0.5 M TEAP recorded during SECM at the 10-μm-diameter Pt UME. Tip currents (I_t) were normalized to the diffusion-limited current recorded at a d of 100 μm ($I_{t,\infty}$). Individual curves were recorded at d values of of (a) >100, (b) 1.6, (c) 0.8, (d) 0.5, and (e) 0.2 μm.

$E_{3/4}$ measurements of steady-state UME voltammograms when UME radius (a), gap size, and diffusion coefficients are known.[47,71]

Table 4 lists values of diffusion coefficients, α_{app}, and $k_{ET,app}$ measured by SECM for the $[M(TCTA)]^{-/0}$ couples in aqueous 0.1 M NH_4ClO_4 (pH 3−4). Increasing the concentration of electrolytes from 0.1 to 1 M yielded < 50% change in apparent rate constants. This insensitivity to ionic strength suggested that electrostatic double-layer effects were relatively small and could be neglected for rate-structure comparisons. Values of $k_{ET,app}$ measured by conventional CV are also included in Table 4 to demonstrate the magnitude of errors that can result without solution resistance corrections. Apparent rate constants measured by SECM were consistently higher than values measured by CV, especially for the faster Fe and Ni couples.

Influence of Structure Change on ET Kinetics. An encounter pre-equilibrium expression (eq 1) for standard adiabatic heterogeneous ET rate constants (k_{ET}) was used

(71) Mirkin, M. V.; Bard, A. J. *Anal. Chem.* **1992**, *64*(19), 2293–2302.

Table 4. ET Kinetic Data (296 K, Pt) with Standard Deviations in Parentheses for $[M(TCTA)]^{-/0/+}$ Redox Couples in Aqueous 0.50 M NH_4ClO_4 (pH 3−4)

M (couple)	$D_{II} \times 10^5$ cm^2 s^{-1}	D_{II}/D_{III}	α_{app}[a]	$k_{ET,app}$ (CV),[b] cm s^{-1}	$k_{ET,app}$ (SECM),[a] cm s^{-1}
$Fe^{III/II}$	1.3	0.99	0.57(6)	0.043(4)	0.57(6)
$Ni^{II/III}$	1.0	1.04	0.36(4)	0.058(8)	0.20(4)
$Mn^{II/III}$	1.2	1.00	0.33(3)	0.0038(2)	0.0048(9)
$Mn^{III/IV}$		(1.0)[c]	0.4(1)	0.032(1)	> 0.1[d]

[a] Measured from $E_{1/4}$, $E_{1/2}$, and $E_{3/4}$ of steady-state SECM voltammograms by using the method of Mirkin and Bard and their tabulations for a uniformly accessible electrode.[55,71] Standard deviations were calculated from voltammograms representing a minimum of five different tip−substrate distances (distance increments > 50% closest distance). [b] Measured from ΔE_p of CVs using the working curve of Nicholson.[72] CVs were recorded with ca. 2 mM solution concentrations of the complexes and sweep rates up to 20 V s^{-1} at a 2-mm-diameter Pt disk electrode.[55] Standard deviations were calculated from CVs representing a minimum of four different sweep rates (sweep rate increments > 50% slowest sweep rate). [c] Diffusion coefficient D_{IV} was not measured. Ratio D_{III}/D_{IV} was assumed. [d] The $Mn^{III/IV}$ wave was overlapped by the quasireversible $Mn^{II/III}$ wave at distances that would have permitted kinetic analysis. The limiting rate constant reflects the highest value measurable at the distance that overlap occurred.

to compare measured rate information to crystallographic estimates of redox-induced structure change.

$$k_{ET} = (K_p \nu_n) \exp\left[\frac{-(\Delta G^*_{is} + \Delta G^*_{os})}{RT}\right] \quad (1)$$

The pre-exponential term in eq 1 is the product of a pre-equilibrium constant (K_p) for the heterogeneous precursor state and a barrier crossing frequency (ν_n) dictated by solvent and reactant harmonic modes, while the exponent terms ΔG_{is}* and ΔG_{os}* are the inner- and outer-sphere activation Gibbs energies, respectively.

Rate-structure comparisons using eq 1 have been carried out for a number of one-electron couples. The approach used in the present work was to estimate inner-sphere reorganization free energies from two sources: crystallographic data and electrochemical rate constants. Gibbs activation energy terms in eq 1 were estimated by assuming a standard dielectric continuum model for the outer-sphere barrier (eq 2):

$$\Delta G^*_{os} = \left(\frac{N}{8}\right)\left(\frac{e^2}{4\pi\varepsilon_o}\right)\left[\frac{1}{r} - \frac{1}{R_e}\right]\left[\frac{1}{\varepsilon_s} - \frac{1}{\varepsilon_{op}}\right] \quad (2)$$

and only metal−ligand bond stretch contributions (a_i) to the crystallographically derived inner-sphere barrier (eq 3):

$$\Delta G^*_{is} = \frac{1}{2}\sum_{i=1}^{2} 3f_i'\left(\frac{\Delta a_i}{2}\right)^2 \quad (3)$$

Equation 2 is the product of three terms, a constant term with the Avogadro's constant (N) and the free space permittivity ($e^2/4\pi\varepsilon_o$), a geometrical term describing the radius (r) of the reactant and the distance (R_e) from its charge image in the electrode, and a solvent-dependent term that reflects different dielectric properties at optical (ε_{op}) and static (ε_s) frequencies. The geometrical term is most uncertain since it assumes a spherical reactant and requires an estimate of the reactant image distance at the point of ET. While $[M(TCTA)]^{-,0,+}$ complexes have a roughly spherical shape with an r of ca. 4.2 Å, the magnitude of the reactant-electrode imaging term ($1/R_e$) is open to question. Because electrode adsorption was not detected for $[M(TCTA)]^{-/0}$ couples under the conditions employed for SECM measurements, the imaging term was probably smaller than $1/r$ and was therefore neglected in the present calculations.

Inner-shell contributions to ET barriers were equated in eq 3 to the energy required to stretch identical M−N bonds ($\Delta a_{i=1}$) and identical M−O bonds ($\Delta a_{i=2}$). Although bond-length changes were available from crystallographic data (Table 3), it was necessary to make estimates of reduced force constants (f') based on averages of experimentally measured force constants.[73−75] M−N(sp^3) force constants were estimated to be 30% higher than M−O(carboxylate) force constants for a particular metal valency and to increase with the oxidation state, with averages being $f_{M(II)-N}$ ca. 76 N m^{-1} and $f_{M(III)-N}$ ca. 180 N m^{-1}. Accordingly, reduced force constants of 110 N m^{-1} (M−N) and 76 N m^{-1} (M−O) were estimated for the $[M(TCTA)]^{-/0}$ couples.

Table 5. Crystallographic[a] and Electrochemical[b] Inner-Sphere Activation Barriers (296 K) for $[M(TCTA)]^{-/0/+}$ Couples

M (couple)	$\Delta G^{\ddagger}_{is,cryst}$ kJ mol^{-1}	$\Delta G^{\ddagger}_{is,echem}$ kJ mol^{-1}
$Fe^{II/III}$	3.1	3.8
$Mn^{II/III}$	(16)[c]	16
$Mn^{III/IV}$	(2.8)[c]	< 8.1
$Ni^{II/III}$	*d*	6.4

[a] Calculated with eq 3 using f'_{M-N} = 110 N m^{-1} and f'_{M-O} = 76 N m^{-1} for $M^{II/III}$ couples and f'_{M-N} = 230 N m^{-1} and f'_{M-O} = 170 N m^{-1} for the $Mn^{III/IV}$ couple. [b] Calculated with eq 1 using $K_p \approx 60$ pm and $\nu_n = 3.2 \times 10^{12}$ s^{-1} as described by Fawcett and Opallo,[13] $\Delta G^{\ddagger}_{os}$ = 22 kJ mol^{-1} (eq 2), and SECM measured rate constants uncorrected for double-layer effects. [c] Values estimated by assuming 78% of $[Mn^{II,IV}(TCTHP)]$ bond length changes occur during $[Mn(TCTA)]^{-/0}$ process. [d] Crystallographic data unavailable.

For the $[Fe(TCTA)]^{0/-}$ couple, the inner-shell activation barriers calculated from crystallographic data using eq 3 closely matched the barrier energy calculated from electrochemical rate constants using eq 1 (Table 5). This correspondence prompted the use of an inner-shell barrier measured by SECM for the $[Mn(TCTA)]^{-/0}$ couple to estimate coordination bond lengths for the crystallographically uncharacterized Mn^{III} species. Cardinal in this estimate was an assumption that structure change of the $Mn^{II/III/IV}$ system occurred in concert with ET and did not involve stable structural intermediates. No such intermediates were observed by fast CV analysis of the $[Mn(TCTA)]^{-/0/+}$ system up to 50 kV s^{-1}.[55] For the estimate, a sufficient percentage of the measured $[Mn(TCTHP)]^{-,+}$ M−N and M−O bond changes were assigned to each Δa_i in eq 3 to match the 16 kJ mol^{-1} electrochemical barrier. Remainders of the M−N and M−O bond changes were then assigned to the $Mn^{III/IV}$ couple. The best match between electrochemical and

(72) Nicholson, R. S. *Anal. Chem.* **1965**, *37*(11), 1351–1355.
(73) Schmidt, K. H.; Müller, A. *Inorg. Chem.* **1975**, *14*(9), 2183–2187.
(74) Schmidt, K. H.; Müller, A. *Coord. Chem. Rev.* **1976**, *19*(1), 41–97.
(75) Kincaid, J. R.; Nakamoto, K. *Spectrochim. Acta, Part A* **1976**, *32*(2), 277–283.

crystallographic barriers was obtained when 78% of $[Mn^{II,IV}(TCHP)]^{-,+}$ structural differences were assigned to the $Mn^{II/III}$ process ($\Delta a_{M-N} = -0.16$ Å and $\Delta a_{M-O} = -0.25$ Å). This structural difference was also in close agreement with M−N and M−O bond length differences between the $[Mn^{II}(TCHP)]^{-}$ and $[Mn^{III}(TCTPr1)]^{0}$ complexes ($\Delta a_{M-N} = -0.12$ Å and $\Delta a_{M-O} = -0.20$ Å).

In a similar manner, structural changes for the $[Ni(TCTA)]^{-/0}$ couple were estimated from the inner-shell barrier measured by SECM. It was not possible in this case to explicitly discriminate between M−N and M−O deformations. However, it seems clear that the significantly greater barrier for the $[Ni(TCTA)]^{-/0}$ couple compared to the $[Fe(TCTA)]^{0/-}$ couple reflects a greater contraction of M−N and M−O bonds with a Ni^{III} center. Such an effect is consistent with the change of one antibonding electron that occurs with the $Ni^{II/III}$ system but not with the $Fe^{II/III}$ system.[19,20]

Conclusions

The $[M(TCTA)]^{-/0}$ couples (M = Mn, Fe, and Ni) appear to be a good homologous series with which to study the effects of mild structural rearrangement on the ET process. Carbonyl stretches observed by FTIR spectroscopy demonstrate that N_3O_3 coordination is preserved in aqueous solution within the pH range of 2−4, and susceptibility measurements indicate little or no interference from spin-state changes. Marcus−Hush expressions for adiabatic ET appear to quantitatively relate structural differences between oxidation states to measured standard heterogeneous electron-transfer rate constants that were uncorrected for double-layer effects. Good correlation was obtained for the Fe couple indicating ΔG_{is*}, ca. 4 kJ mol^{-1}. Structural change associated with the crystallographically undocumented Mn couple was also approximated from electrochemical rate data to be ca. 16 kJ mol^{-1}, a value which corresponded to 78% of the structural difference exhibited between $[Mn^{II,IV}(TCHP)]^{-,+}$ analogs. The moderate inner-sphere ET barriers of these systems compared to their significantly higher outer-sphere barrier (ΔG_{os*}, ca. 22 kJ mol^{-1} in aqueous media) also suggests that $[M(TCTA)]^{-/0}$ couples can provide a favorable range over which to probe the effects of inner-shell vibrations on barrier-crossing dynamics predicted by Marcus and others.[11,25,76]

While accurate measurement of heterogeneous ET rate constants presents a challenge for couples that manifest rapid kinetics, the SECM technique offers several advantages over the conventional method of CV. Foremost, time-based artifacts are not important in SECM since measurements are made under steady-state conditions. Second, high analyte concentrations that are often needed to overcome charging currents at high CV sweep rates are not required for SECM. The 10-fold or greater current enhancements produced by analyte recycling within the SECM gap permits the study of fast ET couples at concentrations below 0.1 mM. This advantage should significantly aid the study of systems over a greater range of solvents and allow greater flexibility in the study of solvent-dependent reactions and dynamical effects on ET kinetics.

Acknowledgment. D.T.P. and T.L.H. acknowledge the donors of the Petroleum Research Fund, administered by the ACS, for partial support of this work and are grateful for grants from 3M Corporation as well as the North Dakota EPSCoR. We also thank Prof. David Wipf for providing a copy of the CE_6000 program.

Supporting Information Available: X-ray crystallographic files, in CIF format, for $[Fe^{II}(H_2O)_6][Fe^{II}(TCTA)]_2$. This material is available free of charge via the Internet at http://pubs.acs.org.

(76) Nadler, W.; Marcus, R. A. *J. Chem. Phys.* **1987**, *86*(7), 3906–3924.